# A General Approach Based on Constrained Parameter-Optimization for the Implicit Representation of Information Concerning Welding Processes

*S.G. Lambrakos and J.O. Milewski*

*(Submitted 27 November 1997; in revised form 6 July 1998)*

**An analysis of weld morphology which typically occurs in deep penetration welding processes using electron or laser beams is presented. The method of analysis is based on geometric constraints with formal mathematical foundation within the theory of constrained parameter optimization. The analysis presented in this report serves as an example of the application of the geometric-constraints method to the analysis of weld fusion boundary morphology where there can be fragmented and incomplete information concerning material properties and only approximate information concerning the character of energy deposition, thus making a direct first principals approach difficult. A significant aspect of the geometric-constraints method is that it permits the implicit representation of information concerning temperature dependence of material properties and of coupling between heat transfer and fluid convection occurring in the weld meltpool.**

**Keywords** complex morphology, constraints, deep penetration, elliptic problem, generating function, parameter optimization

## 1. Introduction

In a series of reports (Ref 1-3) the authors presented a general and flexible approach for the numerical modeling and analysis of dynamic welding processes using a geometric-constraints method that provides a general framework for the inclusion of boundary value information easily obtained from experimental measurements or information based on assumptions (or prior knowledge) concerning the physical character of the welding process. An important feature of this approach for imposing constraints according to boundary value information is that it tends to compensate for either the unavailability of difficult experimental measurements of material properties or gaps in knowledge concerning the characteristics of the energy source. In Ref 1 and 2 the geometric-constraints method was described in terms of its application for the analysis of deep penetration welding processes. In Ref 3 the authors examined the application of the geometric-constraints method to the modeling and analysis of the types of welds that typically result from welding processes such as gas metal arc (GMA), shielded metal arc (SMA), and gas tungsten arc (GTA) welding processes consisting of either single or multiple passes. In addition, Ref 3 provides a relatively extensive survey of mathematical properties related to geometric constraints. The objective of this work is to provide a three-dimensional description of the fusion boundary and associated temperature field. Within sufficient accuracy, this calculation will allow subsequent modeling of heat flow, distortion, and microstructural evolution.

**S.G. Lambrakos,** Materials Science and Technology Division, Code 6324, Naval Research Laboratory, Washington, D.C. 20375-5000; and **J.O. Milewski,** Metallurgy Group, MST-6, Materials Science and Technology Division, Los Alamos National Laboratory, Los Alamos, NM 87545.

In this report the authors present a case study analysis of deep penetration welding of 304 stainless steel for the purpose of further demonstrating the application of their method to these types of welding processes. The specific aspect of the geometric constraints method considered in this report is that it provides a means for the implicit representation of information concerning temperature dependence of material properties and of coupling between heat transfer and fluid convection occurring in the weld meltpool. A model system representing the pseudo steady state of a welding process can be sufficiently specified by a given set of equations, that is, a set of equations representing the physical processes and equations representing constraint conditions, such that inclusion of the Navier-Stokes and continuity equations represents an overspecification of the model system. It is significant to note that this type of overspecification does not pose a formal problem in terms of being incompatible with the geometric-constraints method, which is inherently a method based on constrained parameter-optimization (Ref 4). Overspecification resulting from the inclusion of additional equations can pose problems, however, in terms of large computational requirements and inconvenience with respect to the adjustment of parameters for the purpose of achieving optimization.

In practice, a range of incomplete information exists concerning a given welding process, and characteristics of the pseudo steady state temperature field associated with a given welding process are not conveniently represented mathematically via analytical formulations defined for a closed and bounded solution domain having a relatively simple shape. In practice, the following are among the issues to be considered for modeling a given welding process:

- The total energy input per unit distance for a given welding process may only be known approximately. Factors preventing the precise knowledge of the energy input include energy loss due to vaporization, reradiation, material ejection and loss, laser light reflection, and secondary electron

emission. The combined contribution of these losses is significantly different for various materials being welded under various conditions. Measurements to quantify energy input, such as calorimetry, are slow, expensive, and difficult to perform for processes such as electron beam welding. To the extent that this quantity is known quantitatively, it can provide a global constraint on the three-dimension temperature distribution defined by the pseudo steady state of the weld.

- There can be a lack of information concerning the detailed characteristics of the energy source. Particularly with electron beam and laser welding, but also for arc welding, the characteristics of the energy source are rarely stable and well known. Input parameters can be measured, controlled, and described, but complex interactions with the material surface, for example, keyhole formation, can significantly alter the nature of the effective energy source. Often dynamic instability of the energy source is controlled (by parameter selection) to the extent to which the effect of these instabilities are sufficiently decoupled from the system to result in a consistent stable fusion boundary and resultant weld. As an example, in laser keyhole mode welding, the complex optical reflections occurring within the keyhole, plasma absorption, and focusing of energy, significantly alter the character of the energy source thus making an accurate model of these input conditions extremely difficult.
- The system consisting of workpiece and energy source may not have a simple geometric shape. The top surface of the meltpool may assume a relatively complex shape, which may not be modeled conveniently via mathematical representations that are analytical solutions to the heat-conduction equation defined within domains having shapes characterized by relatively simple geometries.
- The material properties are essentially not constant and can vary substantially as a function of temperature. In addition, the properties of materials at and above the vaporization point are often not contained within the properties database for even common materials.
- Energy transfer within the weld meltpool is coupled to fluid convection and changes in density.

Faced with these difficult issues, it should be repeated that, from a practical point of view, the various types of process information listed above are not the primary goal in understanding and controlling any given process. The primary goal is to understand the geometry of the fusion boundary and thermal state to sufficient accuracy to allow the application of existing modeling tools to predict distortion, microstructural evolution, and material properties.

## 2. Physical Model of the Welding Process

The model system to be specified is that of the dynamic weld in the pseudo steady state. That is to say, the model system is characterized by quasi-steady energy transport in a coordinate system that is fixed in the reference frame of a moving energy source. The outermost boundaries of the model system are defined by the sides of a finite-sized rectangular region. Although the model system is formally that of a general time dependent system, only the pseudo steady state solution is of relevance with respect to geometric-constraint information. In the author's development, the time step and volumetric discretization of the system serve as a means of constructing a weighting sum for the purpose of optimizing the discrete temperature field corresponding to a given set of geometric constraints. The input of energy originating from the energy source is determined in the model system via specification of upstream boundary conditions on closed subdomains located within the specified solution domain. The equations governing the model system are:

$$\rho(T)C_p(T)\frac{\partial T}{\partial t} = \nabla \cdot ([k(T) + k*(\hat{x})]\nabla T) + \nabla \cdot q(T) + \nabla \cdot q(\hat{x}) \quad \text{(Eq 1)}$$

where the quantities $\rho(T)$, $C_p(T)$, and $k(T)$ are the temperature dependent density, heat capacity, and conductivity, respectively, and the temperature-dependent source term $\nabla \cdot q(T)$ is such that

$$\int_t^{t+\tau} \nabla \cdot q(T)dt = \Delta H \quad \text{(Eq 2)}$$

where the quantity $\Delta H$ is the change in energy per unit volume. The quantity $\hat{x} = (x, y, z)$ is the position vector. This method of representing the influence of temperature-dependent source terms is convenient for inclusion into model representations that do not consider time explicitly, for example, the dynamic pseudo steady state of a weld that would occur during a continuous welding process. The source term $\nabla \cdot q(\hat{x})$ is associated with the input of energy into the system resulting from an external energy source. The function $k*(\hat{x})$ represents the influence of the coupling of heat transfer and fluid convection. In the authors' development the temperature-dependent source term $\nabla \cdot q(T)$, the source term $\nabla \cdot q(\hat{x})$, and the modified-conductivity function $k*(\hat{x})$ are considered implicitly via the specification of different types of discrete temperature-field quantities, which are defined in what follows.

## 3. Discrete Representation of Pseudo Steady State Temperature Field

A discrete field representation of the pseudo steady state temperature field can be constructed as follows. First, the solution domain is partitioned into a set of discrete volume elements of volume $(\Delta l)^3$, where each volume element is associated with a node and designated by an index. It is assumed that the node whose index is $p+1$ is located both adjacent and upstream relative to the node whose index is $p$, where $p$ is a positive integer. Second, note that the time interval $\Delta t$ for any position within the workpiece to move a distance $\Delta l$ relative to the energy source is $\Delta l/V_B$. It follows that a consistent discrete representation of Eq 1 is given by:

$$T_p = \frac{1}{(6\kappa_p^* + V_B \Delta l)} \left[ \sum_{i=1}^{6} \kappa_i^* T_i + (V_B \Delta l) T_{p+1} \right] \quad \text{(Eq 3)}$$

where

$$\kappa_i^* = \frac{(\kappa_p + \kappa_i)}{2} \quad \text{(Eq 4)}$$

$$\kappa_p = \frac{1}{6} \sum_{i=1}^{6} \kappa_i \quad \text{(Eq 5)}$$

and

$$\kappa_i = \frac{k_i + k_i^*}{\rho(T_p)\, C_p\,(T_p)} \quad \text{(Eq 6)}$$

The discrete quantities $\kappa_i^*$ defined by Eq 4 are defined such that they represent values of diffusivity, which are functions of discrete positions indexed by $i$ and which are at separations of $\Delta l$ relative to the position whose discrete index is $p$. This strict association of the discrete quantities $\kappa_i^*$ with the discrete positions indexed by $i$, relative to $p$, is significant and concerns formal properties of Eq 3 with respect to constrained parameter optimization. This is discussed in the following paragraphs. The discrete temperature-field quantities $T_i$ (and similarly $T_{p+1}$) are of four types where each provides for the input of specific type of information. Specifically:

$$T_i \text{ and } T_{p+1} = T_D, T_C, T_S, \text{ or } T_E \quad \text{(Eq 7)}$$

where the discrete temperature-field quantities designated by $T_D$ represent those quantities whose values are to be optimized subject (in part) to the constrained or specified values of the discrete temperature-field quantities designated by $T_C$, $T_S$, and $T_E$. The discrete temperature-field quantities designated by $T_C$ represent those quantities with values constrained according to information that is known a priori about the pseudo steady state temperature field associated with a given welding process. The discrete temperature-field quantities designated by $T_S$ represent those quantities with values that are associated with volumetric energy deposition resulting from the energy source term. That is:

$$T_S = T_S[\nabla \cdot q(\hat{x})] = \sum_{n=1}^{M_S} w_n T_n(\hat{x} - \hat{x}_n, \kappa_n) \quad \text{(Eq 8)}$$

The temperature-field quantities designated by $T_E$ are quantities whose values have a special significance in providing a means for the inclusion of information concerning the pseudo steady state temperature field. In contrast to the field quantities designated by $T_C$ and $T_S$, the values of the quantities $T_E$ specify a partitioning of the solution domain into a finite set of subdomains defined by closed boundaries. Accordingly, the temperature field designated by $T_E$ represents boundary values extending over the closed boundaries of these subdomains. These quantities are specified by means of a generation function of the general form:

$$T_E = T_E(\hat{x}) = \sum_{n=1}^{M_E} w_n T_n(\hat{x} - \hat{x}_n, \kappa_n) \quad \text{(Eq 9)}$$

where the functions $T_n$ are Rosenthal type solutions (Ref 5-7) and $w_n$ are weighting functions with a range of values that can in some cases be restricted to only 0 and 1, for example, a unit step or rectangle function. The temperature field quantity designated by $T_E$ provides the means for adjusting the pseudo steady state temperature field at downstream regions. In this sense it assumes a role that is equivalent to that of the quantities designated by $T_S$. It follows then that the solution is driven from both upstream and downstream. It is significant to note that it also provides a mathematical foundation for inversion of experimental measurements for the purpose of extracting information concerning the temperature dependence of material properties (solid and liquid) of the workpiece. Finally, the discrete temperature-field quantities $T_p$ (or equivalently $T_i$ and $T_{p+2}$) spanning the solution domain must satisfy the global constraint condition

$$\frac{(\Delta l)^3}{L} \sum_{p=1}^{N} \int_{T_A}^{T_p} \rho\,(T) C_p(T)\, dT = \frac{q_0}{V_B} \quad \text{(Eq 10)}$$

The quantities $L$ and $q_0$ are the length of the solution domain and total power input, respectively.

An important aspect of the weighted finite sum defined by Eq 3 is that the discrete field quantities $T_i$ and $\kappa_i$ have an equivalent status formally. This property provides the basis for a further extension of the method of geometric constraints. There can be cases where the temperature dependence of the thermal diffusivity $\kappa(T)$ is known only partially. In these cases, for those regions of the solution domain where information concerning the temperature dependence of $\kappa(T)$ is either unavailable or approximate, the discrete diffusivity field $\kappa_i$ can also be adopted as an adjustable discrete field quantity in the same manner as the discrete set of quantities designated by $T_D$. A general requirement for adopting the discrete diffusivity field $\kappa_i$ as an adjustable field quantity is that there exists a sufficient amount of geometric constraint information for assuring (in principle) uniqueness of both the set of quantities $T_i$ (designated by $T_D$) and the set of quantities $\kappa_i$, with temperature dependence that are not known. Further, there can be cases where the amount of available information concerning a weld is sufficiently large that with respect to constrained parameter optimization the system is overconstrained. That is to say, the number of equality constraints of the types designated by $T_C$, $T_S$, and $T_E$ exceeds the number of discrete field quantities with values that are to be optimized. In these cases, an increase in the number of

discrete field quantities can be affected by adopting the quantities $\kappa_i$ as well as $T_i$ for optimization. It follows that the duality property of the quantities $T$ and $\kappa$ associated with the weighted finite-sum representation defined by Eq 3 provides a means for increasing the amount of information that can be included into a model system via constraints.

## 4. Implicit Representation of Temperature-Dependent Material Properties and of the Coupling between Heat Transfer and Fluid Convection

In this section the authors discuss a specific property of constraints that is significant in that it provides a means for including implicitly information concerning the temperature dependence of material properties and information concerning the coupling between heat transfer and fluid convection. In addition, this property provides the basis for a reformulation of the problem in terms of the solution of an elliptic equation defined over a contiguous set of closed subdomains. The mathematical foundation of adopting Eq 3 as an elliptic solver defined over a distributed set of subdomains, while consistently providing implicit representation of the temperature dependence of material and fluid properties follows from an examination of the equivalence between two alternative discrete representations of the problem. One representation is derived from a parabolic equation while the other is from an elliptic equation.

The authors first adopt the assumption that there is sufficient information concerning the downstream region of the pseudo steady state temperature field (for example, information obtained from weld cross sections or thermocouple measurements) and the global morphology of the weld (for example, average three-dimensional shape of meltpool and energy per unit distance) that a specified bounded solution domain can be partitioned into a distributed set of closed subdomains such as are shown schematically in Fig. 1. For a given partitioning of the solution domain into a distributed set of closed subdomains

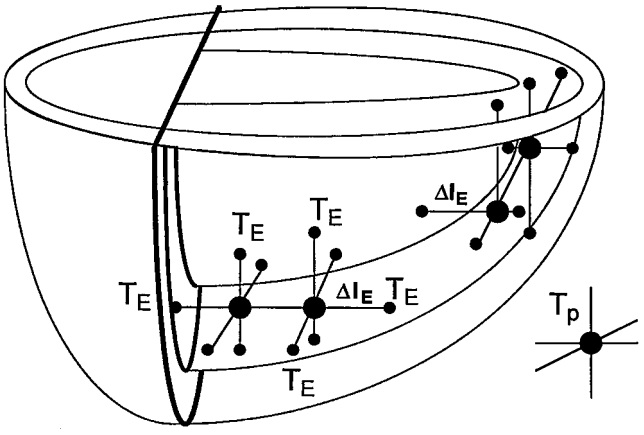


**Fig. 1** Schematic representation of a finite distribution of subdomains providing implicit information concerning the temperature dependence of material properties and of the coupling between energy transfer and fluid convection

(for example, Fig. 1), the authors consider the process of determining a discrete temperature field $T_p$ within each of the closed subdomains. The authors show by means of a partially heuristic proof that for a distributed set of closed subdomains, the weighted finite-sum defined by Eq 3 can be adopted as a consistent elliptic solver for determining the discrete pseudo steady state temperature field. This is based on the property of the temperature-field quantities designated by $T_E$, which specifies the distribution of temperatures over the closed surfaces of the subdomains and which provides for the implicit inclusion of information concerning the temperature dependence of the material properties, the motion of the workpiece relative to the energy source, and of the coupling between heat transfer and fluid convection.

Referring to Fig. 1, it follows by linear interpolation in three dimensions that for a given discrete spatial location $p$ that is located within a given subdomain (upon whose constrained boundaries are assigned the temperature values $T_E$) the discrete temperature field $T_p$ is given by

$$T_p \text{ (inverse problem)} = \sum_{i=1}^{6} W_{E,i}\, T_{E,i} \qquad \text{(Eq 11)}$$

where the weighting coefficients $W_{E,i}$ are functions of the node index $p$ and are given by

$$W_{E,i} = \frac{1}{\Delta l_{E,i}} \left( \sum_{m=1}^{6} \frac{1}{\Delta l_{E,m}} \right)^{-1} \qquad \text{(Eq 12)}$$

and the discrete quantities $\Delta l_{E,i}$, shown in Fig. 1, satisfy the conditions

$$\sum_{i=1}^{6} W_{E,i} = 1 \qquad \Delta l_{E,i} \geq \Delta l \qquad \text{(Eq 13)}$$

where the subdomain containing the node $p$ has been partitioned into a set of discrete volume elements of volume $(\Delta l)^3$. The quantities $\Delta l_{E,i}$ ($i$ = 1, ..., 6) are the distances between a given discrete location within a subdomain (indexed by the integer variable $p$) and its six discrete nearest neighbor locations (indexed by the integer variable $i$), which are on the closed surface of the subdomain. The procedure defined by Eq 11 represents an inverse approach to determining the discrete temperature field $T_p$. That is to say, the procedure for determining $T_p$ is based on the use of prior knowledge concerning only characteristics of the pseudo steady state temperature field and not on any information concerning either the welding process or material properties of the workpiece. It is significant that this distinction is kept clear for a proper interpretation of what follows.

The authors consider next the process of calculating a discrete temperature field $T_p$ over an infinite solution domain for a given set of upstream boundary conditions and a specified flow

field $U$ representing the flow of liquid in the weld meltpool via a direct problem approach. For the purpose of this development the authors adopt a specific representation of the discretization employed by the SIMPLE algorithm (Ref 8), which is defined according to Fig. 2. Accordingly, it follows that given an explicit function $\kappa(T)$, a discrete set of upstream boundary values (or equivalently, an energy source term), top surface and midplane boundary conditions, and a three-dimensional flow field $U$ defined over the region of the meltpool, a unique discrete temperature field is determined according to the weighted sum:

$$T_p(\text{direct problem}) = \frac{1}{6a_p^*} \sum_{i=1}^{6} a_i T_i \qquad \text{(Eq 14)}$$

where the weighting coefficients are defined by:

$$a_i = \kappa_i \max\left[\left(1.0 - 0.1\left|\frac{(\Delta l)(U \cdot I_i)}{\kappa_i}\right|\right), 0\right] + (\Delta l) \max\left[U \cdot I_i, 0\right] + \delta_{i,\,p+1} V_B \Delta l \qquad \text{(Eq 15)}$$

and

$$a_p^* = \frac{1}{6} \sum_{i=1}^{6} a_i \qquad \text{(Eq 16)}$$

The procedure defined by Eq 14, in contrast to that defined by Eq 11, represents a direct problem approach to determining the discrete temperature field $T_p$. That is to say, the procedure for determining $T_p$ is based on either prior knowledge or assumptions concerning only the welding process and material properties of the workpiece and not on any prior knowledge concerning characteristics of the temperature field.

For a given distributed set of subdomains, upon whose surfaces discrete values of $T_E$ are specified, it follows from the condition $T_p$ (direct problem) = $T_p$ (inverse problem) (see Fig. 3) that the equality

$$\sum_{i=1}^{6} W_{E,i}\, T_{E,i} = \frac{1}{6a_p^*} \sum_{i=1}^{6} a_i T_i \qquad \text{(Eq 17)}$$

is satisfied (to within a sufficient level of approximation) with the condition that the discrete temperature field quantities $T_i$ (on the right side of Eq 17) are defined over an open solution domain. The equality expressed by Eq 17 establishes that the volumetrically-distributed values of the field quantity $T_E$ provide an implicit inclusion of information concerning the temperature dependence of material properties and the coupling between heat transfer and fluid flow. The construction defined by Eq 11 represents a linear interpolation of the temperature field $T_E$ over a closed subdomain. It is significant to note that the general form of the sum defined by Eq 11 establishes that Eq 3 can be adopted as a discrete elliptic solver for determining the discrete temperature field within a given closed subdomain. A formal statement of the property that the weighted sum defined by Eq 3 is a discrete elliptic solver for determining $T_p$ (to within a sufficient level of approximation) is that

$$\sum_{i=1}^{6} W_{E,i}\, T_{E,i} = \frac{1}{(6\kappa_p^* + V_B\, \Delta l)}\left[\sum_{i=1}^{6} \kappa_i^*\, T_i + (V_B \Delta l) T_{p+1}\right] \qquad \text{(Eq 18)}$$

for $T_i$ and $T_{p+1}$ within a closed subdomain. A semi-quantitative proof can be constructed that shows that the existence of the sum defined by Eq 11 implies that equality Eq 18 is satisfied. This proof is based on Green's theorem (Ref 9) and is developed in terms of discrete analogs of mathematical representations based on continuous functions and operators. A qualitative and intuitive understanding of the equality Eq 18 follows from the observation that the right side of this equality, applied iteratively over a closed domain, is simply an interpolation among the surface values $T_E$ that bound that domain. A more quantitative proof can be established by means of a reformulation of Eq 3 defined by

$$T_p = \frac{1}{6w_p^*} \sum_{i=1}^{6} w_i^*\, T_i \qquad \text{(Eq 19)}$$

where the weighting coefficients $w_i^*$ and $w_p^*$ are defined by

$$w* = \kappa_i^* + \delta_{i,\,p+1}\,(V_B\, \Delta l) \quad \text{and} \quad w_p^* = \frac{1}{6} \sum_{i=1}^{6} w_i^*; \qquad \text{(Eq 20)}$$

respectively. A significant feature of the formal representation defined by Eq 19, relevant to the authors' development, is that it can be interpreted as the discrete analog of the Laplace equation:

$$\nabla^2[w*\,(T, \hat{x}', V_B)T] = 0 \qquad \text{(Eq 21)}$$

The fact that Eq 3 can be adopted as an elliptic solver, follows from the mathematical properties of elliptic equations, for example, Eq 21.

Given a weighted-temperature field $w*T$, which satisfies the Laplace equation Eq 21 within a given subdomain whose boundary is a closed surface $S$, it follows from Green's theorem (Ref 9) that:

$$w*(T, \hat{x}, V_B)T(\hat{x}) = -\frac{1}{4\pi}\int_S w*(T, \hat{x}', V_B)\, T(\hat{x}')\, \nabla' G(\hat{x}, \hat{x}') \cdot n'\, da' \qquad \text{(Eq 22)}$$

if there is a Green's function $G(\hat{x}, \hat{x}')$ such that:

$$\nabla'^2 G(\hat{x}, \hat{x}') = -4\pi\delta(\hat{x} - \hat{x}') \quad \text{and} \quad G(\hat{x}, \hat{x}') = 0 \qquad \text{(Eq 23)}$$

for positions $\hat{x}$ within the subdomain and positions, $\hat{x}'$, on the surface, *S*, bounding this subdomain. Next, the authors note some properties of $G(\hat{x},\hat{x}')$, which follow from Eq 23. These are:

$$\int_S \nabla' G(\hat{x}, \hat{x}') \cdot n' da' = -4\pi \qquad \text{(Eq 24)}$$

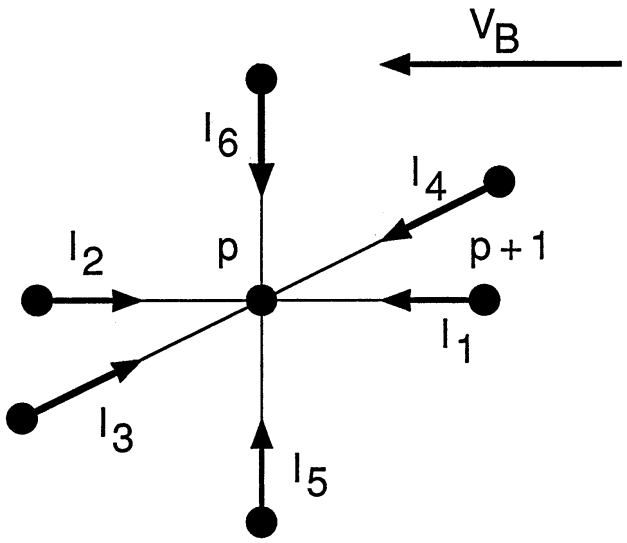


**Fig. 2** Indexing scheme for weighting coefficients $a_i$ defined by Eq 15

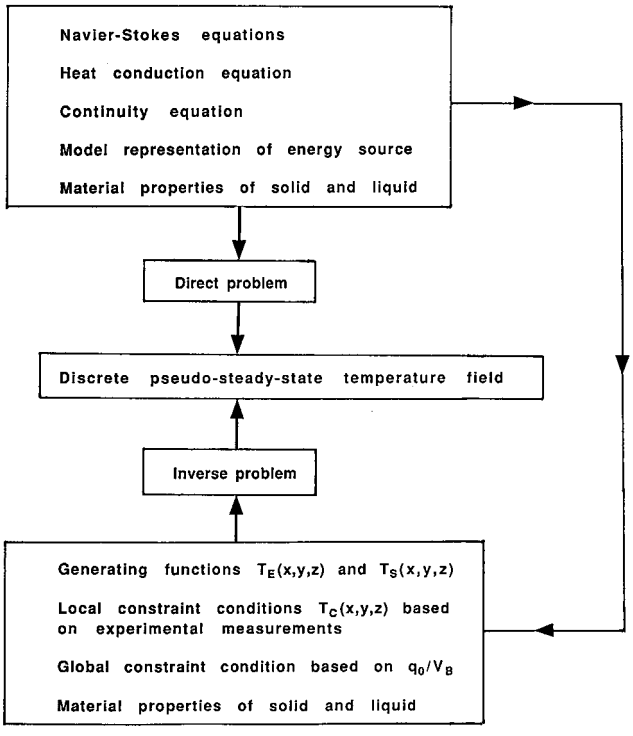


**Fig. 3** Schematic representation of dual interpretation of generation functions $T_E$ and $T_S$ in terms of both direct and inverse problem formalism

and that $G(\hat{x}, \hat{x}')$ is of the general form:

$$G(\hat{x}, \hat{x}') = \frac{1}{|\hat{x} - \hat{x}'|} + F(\hat{x}, \hat{x}') \text{ where } \nabla'^2 F(\hat{x}, \hat{x}') = 0 \qquad \text{(Eq 25)}$$

Equations 22 through 25 provide the general framework for an integral representation of the solution of Eq 21 over a closed domain. Accordingly, construction of a surface integral of the form defined by Eq 22 and of an associated Green's function with properties that are consistent with Eq 23 through 25 implies that the weighted-temperature field $w^*T$ satisfies Eq 21. Next, the authors note that the weighted sum defined by Eq 12 can be interpreted (to within a sufficient approximation) as a discrete analog of Eq 22. That is:

$$-\frac{1}{4\pi}\int_S w^*(T, \hat{x}', V_B)\, T(\hat{x}')\, \nabla' G(\hat{x}, \hat{x}') \cdot n' da'$$

$$= w^*(T_p, \hat{x}, V_B) \sum_{i=1}^{6} W_{E,i}\, T_{E,i} \qquad \text{(Eq 26)}$$

The correspondence represented by Eq 26 establishes the proof. Next, it follows that for a sufficiently dense distribution of contiguous subdomains, the diffusivity function $\kappa(T)$ can vary slowly over the range of temperatures occurring within any given subdomain. It follows then that:

$$\sum_{i=1}^{6} W_{E,i}\, T_{E,i} = \frac{1}{6} \sum_{i=1}^{6} T_i \qquad \text{(Eq 27)}$$

(to within a sufficient level of approximation) for $T_i$ within a closed subdomain, which is sufficiently small that the diffusivity function (which includes in general a modified conductivity) can be assumed effectively constant and that any weighting of the temperature field (which can be due to the motion of the work-

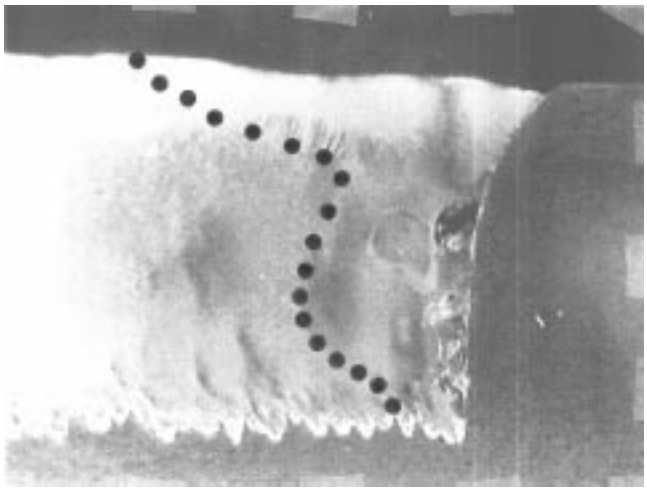

**Fig. 4** Intersection of trailing solidification boundary and symmetry plane parallel to direction of beam travel

piece relative to the energy source, coupling of heat transfer and fluid convection, and the temperature dependence of material properties) can be achieved by the boundary conditions specified by $T_E$ and $T_S$ over the closed surfaces of the set of subdomains.

## 5. Case Study Analysis of Deep Penetration Welding of 304 Stainless Steel

The authors present a case study that is typical of deep penetration welding processes. This analysis serves to demonstrate many features of the geometric constraint method and issues associated with its application in practice. The emphasis of the authors in this report is its application for the analysis of deep penetration welding processes. It is interesting to note that from the standpoint of applying geometric constraints, deep penetration welds represent a relatively simple case. This follows from the inherent character of energy deposition occurring in these processes, which tends to produce overall weld shapes with general features that are simple relative to welds resulting from, for example, GMA welding processes.

For the present case study the authors consider a prototype analysis of the weld, with cross sections that are shown in Fig. 4 and 5 and with process parameters that are given in the Appendix. As shown in these figures, for this analysis three different types of cross sections of the solidification boundary have been adopted for specifying constraints. These are the transverse cross section, the extent of the meltpool at the top surface of the workpiece, and the solidification boundary along the midplane slice of the weld that is parallel to the direction of motion of the beam relative to the workpiece.

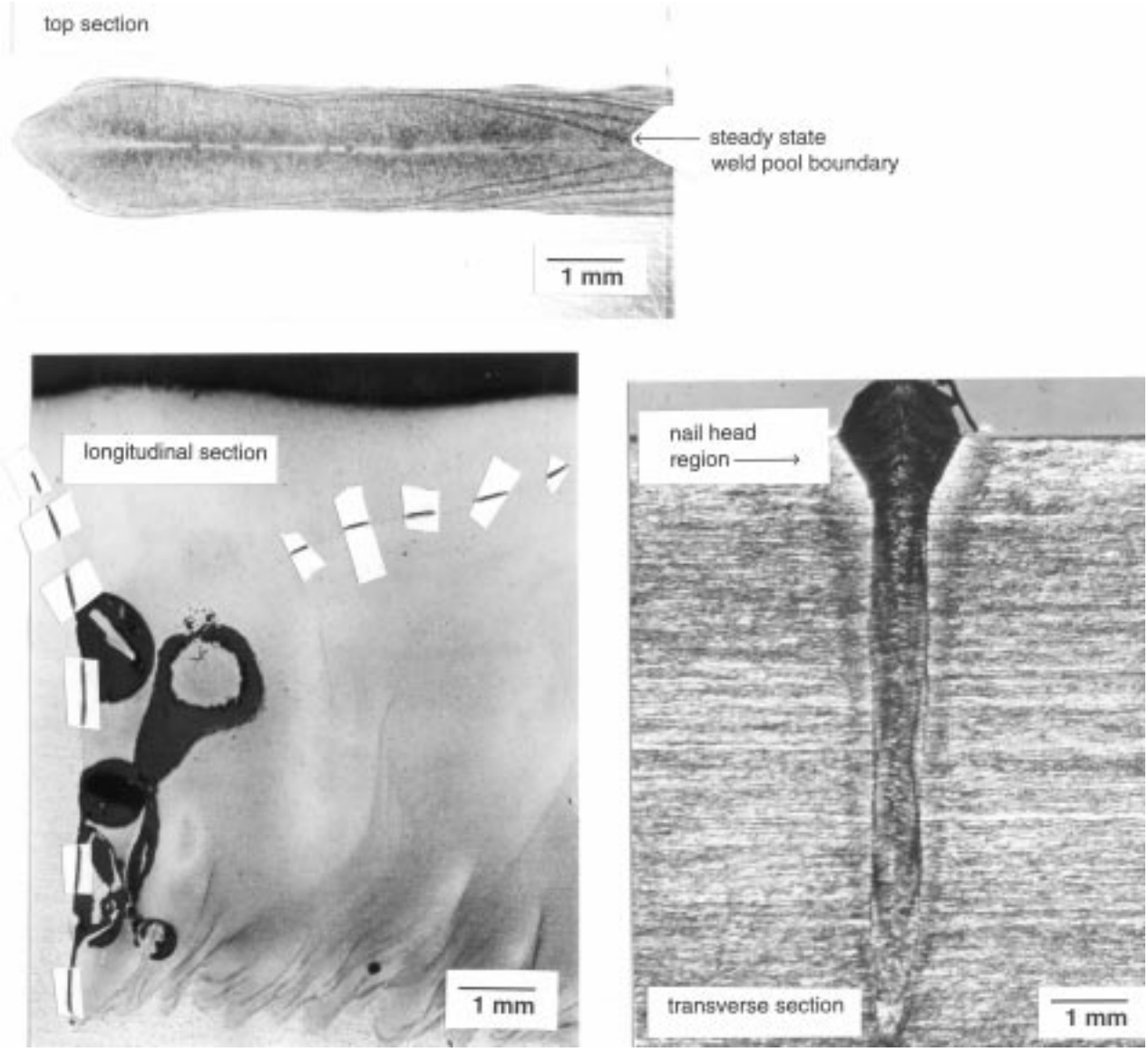


**Fig. 5** Set of experimental cross sections of solidification boundary adopted as constraint conditions on pseudo steady state temperature field

The first stage of the analysis entails the generation of a three-dimensional isothermal surface at $T_M$, with different projections that map onto the experimentally measured cross sections of the solidification boundary (Fig. 4 and 5). This procedure is undertaken by means of a generating function $T_E(\hat{x})$, defined by a line source extending into the solution domain, with magnitude that is a function of the depth of penetration, *z*. The generating function $T_E(\hat{x})$ employed, whose general construction consists of a weighted sum of Rosenthal-type solutions, uses average temperature-independent material properties of steel. These are given in the Appendix.

The second stage of the analysis consists of partitioning the solution domain into a set of closed subdomains. The authors adopt as part of this partitioning the isothermal surface at $T_M$, whose projections onto each of the coordinate planes is consistent with experimental measurements, that is, Fig. 4 and 5. This is again undertaken by means of a line-source generating function $T_E(\hat{x})$. For a grid resolution $\Delta l$ of 0.0794 mm, the solution domain is partitioned into three subdomains. One subdomain is defined by an isothermal surface at $T_G$ (upstream surface), a section of the midplane boundary, a section of the top surface boundary, and the isothermal surface at $T_M$ (downstream surface). A second subdomain is defined by the isothermal surface at $T_M$ (upstream surface) sections of the midplane and top surface boundaries, and the isothermal surface at 850 °C (downstream surface). A third subdomain is defined by the isothermal surface at 850 °C (upstream surface), sections of the midplane and top surface boundaries, and the downstream boundaries of the solution domain.

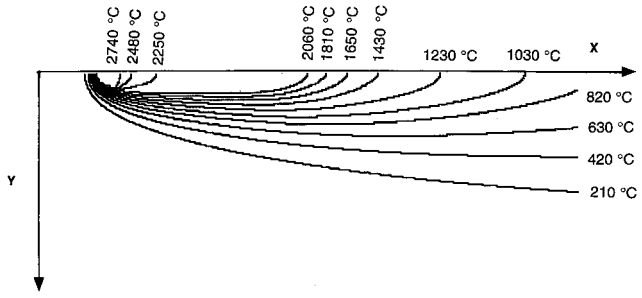


**Fig. 6** Top surface plane at z = 0; two-dimensional slice at top surface of workpiece of three-dimensional temperature field obtained by means of constrained optimization for a grid resolution $\Delta l$ of 0.0794 mm

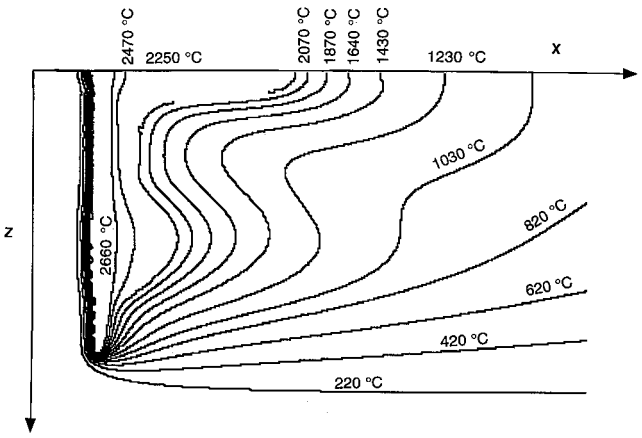


**Fig. 7** Midplane at y = 0; two-dimensional slice at symmetry plane, parallel to direction of beam travel, of three-dimensional temperature field obtained by means of constrained optimization for a grid resolution $\Delta l$ of 0.0794 mm

The third stage of the analysis entails solving Eq 21 over each of the subdomains with the condition that the global constraint condition Eq 10 is satisfied to within a specified tolerance for the entire solution domain. For the subdomain containing the energy source, that is, the subdomain with a closed surface that consists in part of the isotherms $T_M$ and $T_G$, volumetric energy deposition within the workpiece resulting from the energy source is represented by a generating function having a form defined by Eq 8. In the case of deep penetration welding processes, this function has a relatively simple form and can be defined (as in the case of $T_E(\hat{x})$) by a line source extending into the solution domain, whose magnitude is a function of the depth of penetration. Equation 21 is then solved numerically over each closed subdomain by adopting Eq 3 as a discrete field solver for a given grid resolution $\Delta l$. Shown in Fig. 6 and 7 are two-dimensional slices of a three-dimensional temperature field whose discrete values have been determined by solving Eq 21 over the distributed set of subdomains described previously (and in the Appendix). For these calculations the specific set of model parameters, including the grid resolution $\Delta l$ and structure of the set of subdomains, has been adopted such that an optimal temperature field is determined mostly over the subdomain defined by the range of temperatures between 850 °C and $T_M$. The calculated values of the pseudo steady state temperature field that are outside this range are expected to be less optimal but yet sufficient for providing a reasonable estimate of the energy per distance for the welding process, which represents a global constraint on the system. It follows then that a relatively more optimal temperature field can be determined for temperatures greater than $T_M$ by adopting a finer grid resolution and by constructing, via a generating function, a subdomain with temperatures ranging from $T_M$ to 1800 °C, for example. For this calculation values of the temperature field that are outside the range $T_M$ to 1800 °C would be considered relatively less optimal but would still be considered sufficient for contributing to a reasonable estimate of $q_0/V_B$. Similarly, a relatively more optimal temperature field can be determined for temperatures less than 850 °C by adopting a coarser grid resolution and by constructing a subdomain with a downstream boundary defined by an isothermal surface with a temperature less than 850 °C. This procedure also represents the basic approach for extending the total range of values for the calculated temperature field. In order to demonstrate this approach the authors now present a repetition of the constrained optimization procedure using a grid resolution that is approximately twice that adopted for the calculation of the temperature field shown in Fig. 6 and 7. In the course of this presentation the authors examine various general features of the calculation.

Shown in Fig. 8(a) and (b) are two-dimensional slices of a three-dimensional temperature field whose values have been determined by means of a generating function. The only condition imposed on this field is that the three-dimensional isother-

mal surface at $T_M$ consistently map onto the experimentally measured cross sections, that is, Fig. 4 and 5. Referring to Fig. 8(b), it is seen that the general character of the temperature field at regions close to the top surface boundary of the solution domain is not physically realistic or consistent with the general influence of surface boundary conditions.

Shown in Fig. 9(a) and (b) are two-dimensional slices of a three-dimensional temperature field with discrete values determined by solving Eq 21 over a distributed set of subdomains. Referring to Fig. 9(b), it can be seen that the general character of the temperature field is physically realistic at regions near to and at the top surface boundary of the solution domain. An interesting aspect of the optimization procedure to note here is that optimization of the temperature field can be undertaken over subdomains with intersecting regions. This aspect of the procedure actually helps in providing more convenience with respect to optimization of the temperature field. For this calculation, corresponding to a grid resolution $\Delta l$ of 0.159 mm, the solution domain is partitioned into the set of subdomains (some of which are mutually overlapping) with upstream and downstream boundaries listed in the Appendix. Each subdomain is defined by an upstream boundary, a downstream boundary, a section of the midplane boundary, and a section of the top surface boundary. The temperature field of the top surface and midplane slices shown in Fig. 9(a) and (b) is the result of a two-step calculation. The first step consists of solving Eq 21 over the set of subdomains defined by the set of temperatures ($T_G$, $T_M$, 1800 °C, 850 °C, and 650 °C) and by adopting the temperature field calculated by means of the function $T_E(\hat{x})$ (Fig. 8a and b) as an initial estimate. The second step consists of adopting the temperature field resulting from the first step as an initial estimate and then solving Eq 21, sequentially, over the set of subdomains with upstream and downstream boundaries defined by the isothermal surfaces given by the ordered pairs (1700 °C, 1200 °C), (1000 °C, 650 °C), and (700 °C, 600 °C).

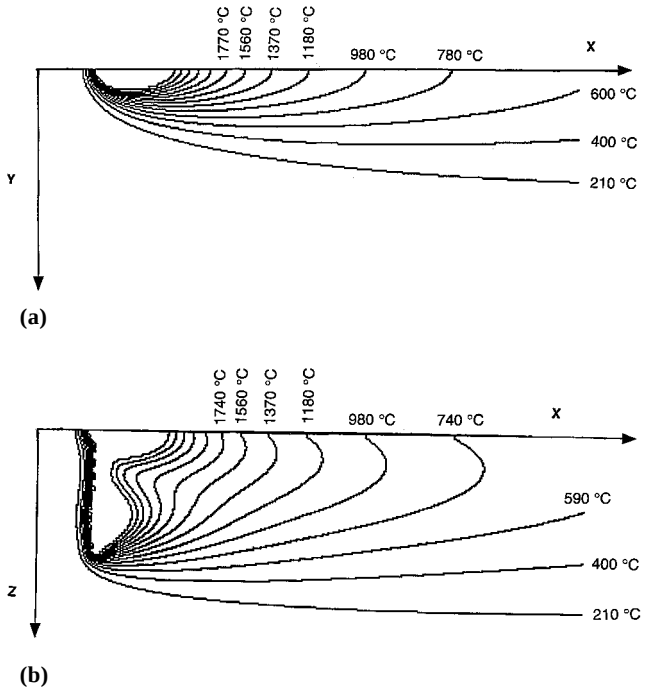


**Fig. 8** (a) Top surface plane at z = 0; two-dimensional slice at top surface of workpiece of three-dimensional temperature field obtained by means of a generating function. (b) Midplane at y = 0; two-dimensional slice at symmetry plane, parallel to direction of beam travel, of temperature field obtained by means of a generating function

The authors next consider optimization with respect to material properties. Before discussing this issue, however, a brief review of specific aspects of their approach is in order. For a given grid resolution $\Delta l$, the constrained optimization procedure, representing the practical application of the method of geometric constraints, consists of the determination of a progression of successively improved estimates of the pseudo steady state temperature field. Local adjustment of a given temperature field (serving as a prior estimate) for the purpose of including additional information concerning the weld (and thus improving the estimate) is achievable (conveniently) because of the properties associated with partitioning of the solution domain into subdomains. In the case study analysis presented here, an initial estimate of the temperature field is calculated via a generating function $T_E(\hat{x})$, which assumes temperature-independent material properties. This represents a relatively convenient approach for calculating a prior estimate of the pseudo steady state temperature field. It is significant to note (as described schematically by Fig. 3), that, as a prior estimate, a temperature field resulting from a calculation based on a relatively detailed model representation of the welding process can be adopted. This could be, for example, a model representation which includes equations representing the fluid flow in the melt pool and the temperature dependence of the material properties. In the present analysis, information concerning the temperature dependence of the material properties of 304 stainless steel (Ref 10) was included during the optimization procedure, which consisted of solving Eq 21 over individual subdomains for a given specification of the discrete weighting functions defined by Eq 20.

In the present study, optimization with respect to total energy input is achieved by adjustment of the temperature field according to the condition defined by Eq 10. For the discrete temperature fields calculated, the sum on the left side of Eq 10 was found to have values of $1.58 \times 10^5$ J/m and $1.5 \times 10^5$ J/m for grid resolutions $\Delta l$ of 0.0794 and 0.159 mm, respectively. These calculated estimates of the energy input per distance are somewhat greater than the experimentally determined maximum energy input possible for coupling into the workpiece (see the Appendix). In order to adopt the quantity $q_0/V_B$ as a strict constraint condition, it is necessary to relax other constraint conditions so that the system is not overconstrained. Adopting the condition $q_0/V_B = 1.0 \times 10^5$ J/m as a relatively strict constraint, the authors consider the relaxation of the constraint conditions associated with the longitudinal midplane shape of the solidification boundary (that is, Fig. 4) and the effective maximum (time-averaged) temperature distribution characterizing the deep penetration energy source. The relaxation of these constraints could be based on the following physical arguments. First, the shape profile shown in Fig. 4 represents an estimate of the pseudo steady state shape of the solidification boundary obtained by means of a specific etching

procedure (see Ref 2). It is plausible to assume that this shape feature should be adopted as an approximate constraint rather than in a shape constraint that should be strictly satisfied. Second, it is observed experimentally that the vapor-liquid interface, which defines the keyhole (a characteristic feature of deep penetration welding processes), tends to be an unstable structure that collapses and then reforms quasi periodically. It follows then that the effective maximum temperature distribution characterizing the steady-state energy deposition resulting from a deep penetration welding process (a time-average quantity) could be significantly less than the vaporization temperature $T_G$. Shown in Fig. 10(a) and (b) are two-dimensional slices of a three-dimensional temperature field with discrete values determined following the authors' optimization procedure. For the discrete temperature fields calculated, the sum on the left side of Eq 10 was found to have a value of $1.15 \times 10^5$ J/m for a grid resolution $\Delta l$ of 0.159 mm. As shown in these figures, the strict condition on the quantity $q_0/V_B$ can be achieved by adopting an average effective temperature of 2000 °C in the region containing the energy source and by relaxing the condition defined by the dynamic shape feature of the solidification boundary shown in Fig. 4. It should be noted that the representation of the energy source via an average temperature distribution is not inappropriate for this specific calculation because the authors have adopted a grid resolution and domain partitioning that are suitable for optimizing the calculated temperature field at regions that are downstream and relatively far removed with respect to the location of the energy source, for example, temperatures less than 800 °C. A consistent approach for optimizing the temperature field for regions close to and including the energy source (and maintaining the global constraint condition on $q_0/V_B$) would entail adopting a finer grid resolution and a local set of subdomains bounding the energy source (within which there would be a grid of sufficiently finer resolution) such that the optimized temperature field averaged over this set of subdomains has a value of approximately 2000 °C. In principle, this calculation would entail more detailed information concerning the time-average temperature distribution characterizing the energy deposition, that is, the quantities $T_S$ defined by Eq 8.

It has been shown here, however, that the easily obtainable geometric constraint information, which would normally be available during the course of a typical weld analysis, such as metallographic cross-section data, can be used to help calculate a temperature field for a high energy density weld. A key point is that this temperature field was calculated without in depth knowledge of the energy source and only approximate information regarding the total energy input, material properties,

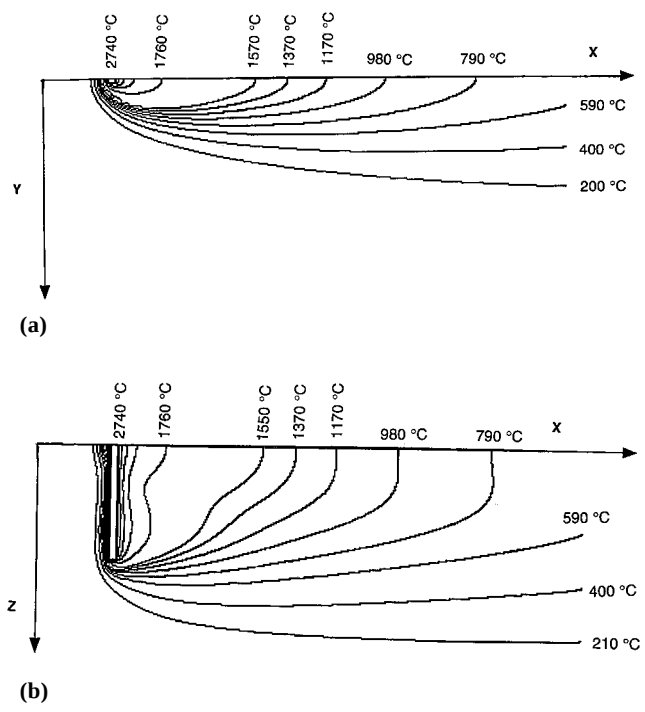


**Fig. 9** (a) Top surface plane at z = 0; two-dimensional slice at top surface of workpiece of three-dimensional temperature field obtained by means of constrained optimization for a grid resolution $\Delta l$ of 0.159 mm. For this calculation the shape shown in Fig. 4 is accepted as a strict constraint condition. (b) Midplane at y = 0; two-dimensional slice at symmetry plane, parallel to direction of beam travel, of temperature field obtained by means of constrained optimization for a grid resolution $\Delta l$ of 0.159 mm. For this calculation the shape shown in Fig. 4 is accepted as a strict constraint condition.

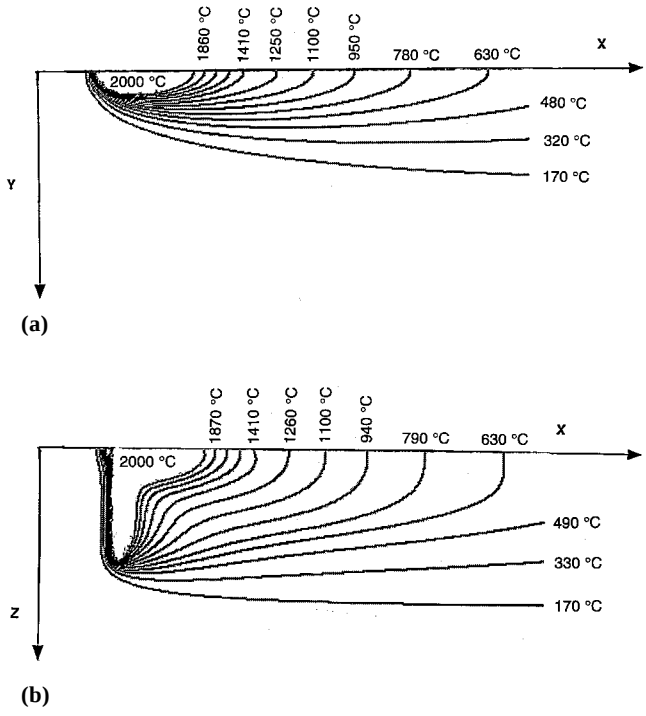


**Fig. 10** (a) Top surface plane at z = 0; two-dimensional slice at top surface of workpiece of three-dimensional temperature field obtained by means of constrained optimization for a grid resolution $\Delta l$ of 0.159 mm. For this calculation the condition $q_0/V_B$ = 100 kJ/m is accepted as a strict constraint condition. (b) Midplane at y = 0; two-dimensional slice at symmetry plane, parallel to direction of beam travel, of temperature field obtained by means of constrained optimization for a grid resolution $\Delta l$ of 0.159 mm. For this calculation the condition $q_0/V_B$ = 100 kJ/m is accepted as a strict constraint condition.

and energy transfer within the melt region. Further validation of the model, particularly for larger more complex shaped weld pools, such as those obtained using arc welding, using techniques such as impulse decanting to determine the shape of the fusion boundary are left for future work. Advanced sensing methods such as noncontact thermography may provide additional easily obtainable constraint information with which the accuracy of the model can be improved.

## 6. Conclusions

The method of geometric constraints has been examined in terms of its ability to provide an approach for the implicit representation of information concerning welding processes. A case study has been presented for the purpose of demonstrating the application of this method in the analysis of deep penetration welding processes. These types of welding processes are characterized by relatively simple shape features in contrast to other types of welding processes where the fusion zone can be characterized by a complex morphology, for example, GMA processes consisting of either single or multiple passes. The mathematical foundation of the geometric constraints method is that of constrained optimization of a discrete parameter system. Following this method, the solution is driven equally from both upstream and downstream boundaries. This is in contrast to the standard approach of associating all parameterization with upstream regions of the weld. The problem is posed as a discrete optimization problem over a distributed set of closed subdomains where all boundaries are given equal weighting and where boundary values, both upstream and downstream, represent the input of information into the model system. The formal mathematical distinction of the authors' approach is that it casts the dynamic weld problem as an elliptic problem. Although their approach is based on parameter optimization in the strict sense, it does not concern the optimization of any parameters associated with a physical model representation of the dynamic weld. In general, no parameterization of the model system is assumed beyond that of a finite set of temperatures, conductivities, and diffusivities, that is, $\{T_p, k_p, \kappa_p\}$, where $p = 1, ..., N_S$. Any parameterization associated with the generating functions, $T_S(\hat{x})$ or $T_E(\hat{x})$, represents only an estimate and must not be interpreted as either a parameterization of the system or a characterization of the energy source. Accordingly, the energy input per distance $q_0/V_B$ is not to be interpreted as a parameter but rather as a global constraint on the system.

## 7. Appendix

**Material properties used for generating functions**

$T_M = 1426.85$ °C
$k = 25$ W/mC
$\rho C_p = 5 \times 10^6$ J/m$^3C$
$\kappa = 5 \times 10^{-6}$ m$^2$/s
$T_G = 2741.0$

**Welding parameters for electron beam weld**

| Parameter | Value |
|---|---|
| Weld speed ($V_B$), m/s | $3.0 \times 10^{-2}$ |
| Average energy input per distance ($Q/D$), kJ/m | 100 |
| Bead depth below surface, mm | 8.0 |
| Bead width at surface, mm | 1.66 |
| Plate thickness, m | 0.0254 |
| Power input [$(Q/D)V_B$], W | $3.0 \times 10^3$ |
| Maximum possible power input, W | $3.75 \times 10^3$ |

**Domain partitioning for grid spacing $\Delta l = 0.7938 \times 10^{-4}$ m**
See Fig. 6 and 7

| Upstream boundary | Downstream boundary |
|---|---|
| $T_G$ | $T_M$ |
| $T_M$ | 1800 °C |
| 1800 °C | 850 °C |

**Domain partitioning for grid spacing $\Delta l = 1.59 \times 10^{-4}$**
See Fig. 9(a) and (b)

| Upstream boundary | Downstream boundary |
|---|---|
| $T_G$ | $T_M$ |
| $T_M$ | 1800 °C |
| 1800 °C | 850 °C |
| 850 °C | 650 °C |
| 1700 °C | 1200 °C |
| 1000 °C | 650 °C |
| 700 °C | 600 °C |


### Acknowledgment

The authors would like to thank Mr. Harry N. Jones III for his discussions concerning welding processes.


### References


1. S.G. Lambrakos, E.A. Metzbower, J. Milewski, G. Lewis, R. Dixon, and D. Korzekwa, *J. Mater. Eng. Perform.,* Vol 3 (No. 5), 1994, p 639
2. S.G. Lambrakos and J. Milewski, *J. Mater. Eng. Perform.*, Vol 4 (No. 6), 1995, p 717
3. S.G. Lambrakos and D.W. Moon, in GORDON and BREACH International Series in Engineering, Technology, and Applied Science Volumes on "Computer Aided and Integrated Manufacturing Systems Techniques and Applications"
4. G.R. Walsh, *Methods of Optimization,* John Wiley & Sons Ltd., London, 1975
5. D. Rosenthal, *Weld. J. Res. Suppl.*, Vol 20, 1941, p 220
6. D. Rosenthal, *Trans. ASME,* Vol 68, 1946, p 849
7. H.S. Carslaw and J.C. Jaeger, *Conduction of Heat in Solids,* 2nd ed., Oxford, 1959
8. S.V. Patankar, *Numerical Heat Transfer and Fluid Flow,* Hemisphere Publishing, 1980
9. J.D. Jackson, *Classical Electrodynamics*, John Wiley & Sons, 1962, p 15
10. T. Zacharia and S.A. David, *Mathematical Modelling of Weld Phenomena*, H. Cerjack and K.E. Easterling, Ed., Institute of Materials, London, 1993